

## Search for Ultralight Dark Matter with Quantum Magnetometry in the Earth's Cavity

Ariel Arza,<sup>1,2,\*</sup> Yuanlin Gong,<sup>1,\*</sup> Jun Guo,<sup>3,\*</sup> Xiaofei Huang,<sup>4,\*</sup> Jing Shu,<sup>5,6,7,†</sup> Hongliang Tian,<sup>1</sup> Wenyu Wang,<sup>8</sup> Kai Wei,<sup>9,4,‡</sup> Lei Wu,<sup>1,2,§</sup> Mingming Xia,<sup>10</sup> Jin Min Yang,<sup>11,12</sup> Qiang Yuan,<sup>13,14</sup> Yang Zhang,<sup>11,\*</sup> Yi Zhang,<sup>13,14</sup> and Bin Zhu<sup>15,¶</sup>

<sup>1</sup>Department of Physics and Institute of Theoretical Physics,
Nanjing Normal University, Nanjing, 210023, China
<sup>2</sup>Nanjing Key Laboratory of Particle Physics and Astrophysics, Nanjing, 210023, China
<sup>3</sup>College of Physics and Communication Electronics,
Jiangxi Normal University, Nanchang 330022, China

<sup>4</sup>School of Instrumentation and Optoelectronic Engineering, Beihang University, Beijing 100191, China <sup>5</sup>School of Physics and State Key Laboratory of Nuclear Physics and Technology, Peking University, Beijing 100871, China <sup>6</sup>Center for High Energy Physics, Peking University, Beijing 100871, China

<sup>7</sup>Beijing Laser Acceleration Innovation Center, Huairou, Beijing, 101400, China
 <sup>8</sup>Beijing University of Technology, 100124, Beijing, China
 <sup>9</sup>Quantum Science and Technology College, Beihang University, Beijing 100191, China

Hangzhou Institute of Extremely-Weak Magnetic Field Major National
 Science and Technology Infrastructure, Hangzhou, 310051, China
 Center for Theoretical Physics, Henan Normal University, Xinxiang 453007, China
 Institute of Theoretical Physics, Chinese Academy of Sciences, Beijing 100190, China
 Key Laboratory of Dark Matter and Space Astronomy,

Purple Mountain Observatory, Chinese Academy of Sciences, Nanjing 210023, China

14 School of Astronomy and Space Science, University of Science and Technology of China, Hefei 230026, China

15 School of Physics, Yantai University, Yantai 264005, China

Ultralight dark matter candidates, such as axions and dark photons, are leading dark matter candidates. They may couple feebly to photons, sourcing oscillating electromagnetic signals in the presence of magnetic field. The Earth resonant cavity formed between the ground and the ionosphere provides a natural waveguide that can amplify such signals. We carry out a project aiming to search for new physics using the unshielded high-sensitivity atomic magnetometer, termed the Geomagnetic Probe for nEw physiCS (GPEX). In this work, we report our first search for axion and dark photon dark matter, conducted in the desert of XiaoDushan in Gansu Province, China. Analysis of the collection of one-hour data shows no evidence for axion- or dark photon-induced magnetic signals. Correspondingly, we set the constraints on the axion-photon coupling with  $g_{a\gamma\gamma} < 7 \times 10^{-10} \, {\rm GeV}^{-1}$  and the dark photon kinetic-mixing parameter  $\epsilon < 2 \times 10^{-6}$  in the mass range  $3.5 \times 10^{-16} \, {\rm eV} \sim 1.8 \times 10^{-14} \, {\rm eV}$ . Our findings demonstrate the feasibility of using ground-based quantum magnetic sensors for ultralight dark matter searches. Future networks of such detectors operating over extended periods could further enhance sensitivity, approaching the limits set by astrophysical observations.

Introduction. Cosmological observations indicate that only about 16% of the universe's total matter is baryonic. While the Standard Model of particle physics accurately describes this component, the nature of the remaining ~84%—the enigmatic dark matter—remains a fundamental problem at the intersection of particle physics, cosmology, and astrophysics [1]. Consequently, leading dark matter candidates now arise from extensions to the Standard Model that introduce ultralight fields, such as axions, axion-like particles, and dark photons [2–7].

The axion, originally proposed to solve the strong-CP problem in quantum chromodynamics [8], also emerges naturally in high-energy frameworks such as string theory and extra-dimensional models [9–11]. Another promising candidate, the dark photon, provides a portal to the dark sector through kinetic mixing with the Standard Model photon [5, 12–15]. A key cosmological virtue of these ultralight fields is that they can be produced in the early

universe via non-thermal mechanisms, naturally accounting for the observed dark matter relic density [2–6, 16].

Ultralight dark matter (ULDM), with masses ranging from  $10^{-22}$  eV to a few eV, behaves as a weakly coupled, coherent classical field that permeates all space. Probing ultralight axions and dark photons relies on their non-gravitational couplings to Standard Model particles [17–32]. Consequently, a suite of specialized experimental approaches has been developed to probe their couplings to the photon field. These include shielded experiments such as ADMX [21], DM-Radio [33], ABRA-CADABRA [34], and others [31, 35–37]. On the other hand, experiments involving quantum sensing and their networks, such as atomic spectroscopy [38], superconducting cavities [39–44], atomic magnetometers [29, 45], state-swapping techniques [46–49], and squeezed-state receivers [50], have achieved unprecedented sensitivities. These advances are attributed to their ability to enhance the effective sensitivity of the sensors and to confidently

distinguish signals from various sources of noise using correlated data.

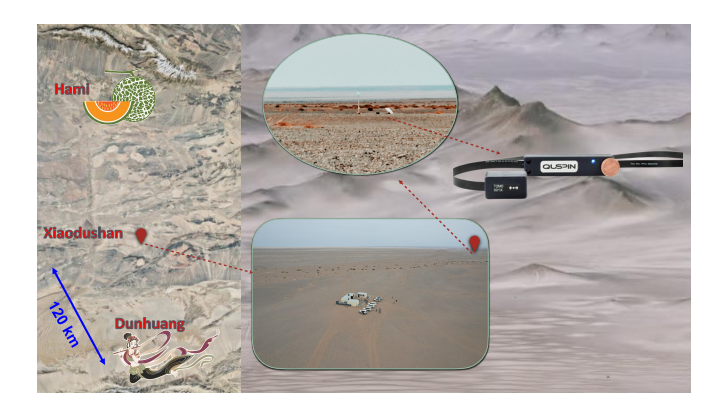


Figure 1. Setup for our experiment. Away from the Dunhuang city 120 km, in the desert of XiaoDushan, we made our one-hour high performance measurement using the QTFM-B scalar atmoic magnetometer.

In this work, we utilize an unshielded atomic magnetometer—an optically pumped rubidium magnetometer—to conduct the Geomagnetic Probe for EXotic physics (GPEX), targeting dark matter axions and dark photons. The experiment was carried out in the desert of XiaoDushan, Gansu Province, China, a location far from anthropogenic electromagnetic noise. By leveraging the Earth as a giant transducer, the natural conducting cavity formed by the Earth's surface and ionospheric layers facilitates the conversion of ultralight dark matter fields into detectable magnetic field signals. This enhancement is particularly effective for ultralight axion and dark photon fields with Compton wavelengths comparable to or larger than the Earth's size, corresponding to a mass range of  $3.5 \times 10^{-16} \,\text{eV} \sim 1.8 \times 10^{-14} \,\text{eV}$ , where the Earth's radius  $R_e \gg L$  (with L being the characteristic size of the field oscillation). We analyze one hour of data collected using our high-sensitivity quantum magnetometer and identify no robust signal candidates from dark matter axions and dark photons. Based on this null result, we derive constraints on the axionphoton coupling  $g_{a\gamma\gamma}$  and the dark photon kinetic mixing parameter  $\epsilon$  within the specified mass range. Owing to the exceptional sensitivity of the magnetometer and the quiet experimental environment, our limits reach  $g_{a\gamma\gamma} \sim 7 \times 10^{-10} \, \text{GeV}^{-1}$  and  $\epsilon \sim 2 \times 10^{-6}$ . These results demonstrates the strong potential of unshielded atomic magnetometers for rare event searches.

Theoretical background. Ultralight dark matter can interact feebly with electromagnetic fields. Because its occupancy number is extremely high, the dark matter field behaves classically. This collective effect can be incorporated into Maxwell's equations as an effective classical current  $\vec{J}_{\rm DM}$ , which acts as a source for electromagnetic phenomena. In this context, the phenomenology is

reduced to solve the classical equations [36]

$$\vec{\nabla} \cdot \vec{E} = 0 \tag{1}$$

$$\vec{\nabla} \cdot \vec{B} = 0 \tag{2}$$

$$\vec{\nabla} \times \vec{E} = -\partial_t \vec{B} \tag{3}$$

$$\vec{\nabla} \times \vec{B} = \partial_t \vec{E} + \vec{J}_{\rm DM} , \qquad (4)$$

where  $\vec{B}$  and  $\vec{E}$  are the magnetic and electric fields, respectively. Effective dark matter charge densities are suppressed by the dark matter velocity.

We use spherical coordinates  $\vec{x} = (r, \theta, \varphi)$  and expand the effective current  $\vec{J}_{\rm DM}$  in series of vector spherical harmonics (VSH),  $\vec{Y}_{\ell m}$ ,  $\vec{\Psi}_{\ell m}$  and  $\vec{\Phi}_{\ell m}$  as

$$\vec{J}_{\mathrm{DM}}(\vec{x},t) = e^{-i\omega t} \sum_{\ell,m} \left( J_{\ell m}^{(r)}(r) \vec{Y}_{\ell m}(\theta,\varphi) + J_{\ell m}^{(1)}(r) \vec{\Psi}_{\ell m}(\theta,\varphi) \right)$$

$$+J_{\ell m}^{(2)}(r)\vec{\Phi}_{\ell m}(\theta,\varphi)$$
 , (5)

where  $\ell=0,1,2,\ldots$  and  $m=-\ell,-\ell+1,\ldots,\ell-1,\ell$ . The parameter  $\omega$  corresponds to the typical angular frequency of the system, which is equivalent to the dark matter particle masses  $m_a$  and  $m_{\gamma'}$  for axions and dark photons respectively. For ultralight fields such as axions and dark photons, the identity  $\vec{\nabla} \times \vec{J}_{\rm DM} = 0$  is satisfied. From VSH properties, it is implied directly that  $J_{\ell m}^{(2)} = 0$ , and that  $J_{\ell m}^{(r)} = r J_{\ell m}^{(1)\prime} + J_{\ell m}^{(1)}$ . We look for magnetic field solutions at the Earth's surface, considering that electromagnetic fields are bounded on the one side by the ground and on the other side by the ionosphere. For Compton wavelengths bigger than the ionosphere height, the dark matter induced magnetic field signal  $\vec{B}_{\rm DM}$  at the Earth's surface is determined uniquely by the radial component  $J_{\ell m}^{(r)}$  of the effective current. We find

$$\vec{B}_{\rm DM}(\theta, \varphi, t) = -e^{-i\omega t} \sum_{\ell, m} \frac{R_e J_{\ell m}^{(r)}(R_e) \vec{\Phi}_{\ell m}(\theta, \varphi)}{\ell(\ell+1) - \omega^2 R_e^2} ,$$
 (6)

where  $R_e = 6371.2 \,\mathrm{km}$  is the Earth's radius. The divergences shown in Eq. (6) correspond to Schumann resonances. These resonances are not discussed in this work since the target parameter space satisfies  $\omega^2 R_e^2 < 2$ .

For axions, the effective current at  $r = R_e$  is [51]

$$\vec{J}_a = ig_{a\gamma\gamma} m_a a_0 e^{-im_a t} \sum_{\ell,m} C_{\ell m} \left( (\ell+1) \vec{Y}_{\ell m} - \vec{\Psi}_{\ell m} \right) ,$$
(7

where  $g_{a\gamma\gamma}$  is the axion-photon coupling constant,  $a_0$  the complex axion amplitude, normalized by  $\frac{1}{2}m_a^2\langle |a_0|^2\rangle = \rho_0$ , where  $\rho_0$  is the local dark matter energy density which in this work is taken as  $0.3\,\mathrm{GeV/cm}^3$ . The coefficients  $C_{\ell m}$  are taken from the IGRF-13 model of the Earth's geomagnetic field [52]. By comparing Eq. (7) with the general expression in Eq. (5), the radial component  $J_{\ell m}^{(r)}$ 

of the effective current is identified, thus the axion signal is computed as

$$\vec{B}_{a} = -ig_{a\gamma\gamma}m_{a}R_{e} \, a_{0} \, e^{-im_{a}t} \sum_{\ell,m} \frac{(\ell+1)C_{\ell m}\vec{\Phi}_{\ell m}(\theta,\varphi)}{\ell(\ell+1) - m_{a}^{2}R_{e}^{2}} \, .$$
(8)

For dark photons, the effective current is given by [53]

$$\vec{J}_{\gamma'} = -\sqrt{\frac{4\pi}{3}} \epsilon m_{\gamma'}^2 \sum_{m=-1}^{1} A'_m \left( \vec{Y}_{1m} + \vec{\Psi}_{1m} \right) e^{-i\omega_m t} , \quad (9)$$

where  $\epsilon$  is the kinetic mixing parameter between dark photons and standard model photons and  $A'_m$  the dark photon amplitudes defined in terms of  $\vec{A}' = (A'_x, A'_y, A'_z)$  as  $A_1 = -\frac{1}{\sqrt{2}}(A'_x - iA'_y)$ ,  $A_1 = \frac{1}{\sqrt{2}}(A'_x + iA'_y)$  and  $A'_0 = A'_z$ , where  $\vec{A}'$  is normalized as  $\frac{1}{2}m_{\gamma'}^2 \left\langle |\vec{A}|^2 \right\rangle = \rho_0$ . For dark photons, the oscillation frequency is defined as  $\omega_m = m_{\gamma'} - 2\pi m f_d$ , where  $f_d$  is the frequency associated to the sidereal day, which accounts for the effects of Earth's rotation. As the data used in this work correspond to a couple of hours, we neglect Earth's rotation effects. Just like in the axion case, we identify  $J_{\ell m}^{(r)}$  in Eq. (9) and find a dark photon magnetic field signal given by

$$\vec{B}_{\gamma'} = \sqrt{\frac{4\pi}{3}} \frac{\epsilon m_{\gamma'}^2 R_e}{2 - m_{\gamma'}^2 R_e^2} e^{-im_{\gamma'}t} \sum_{m=-1}^1 A_m' \vec{\Phi}_{1m}(\theta, \varphi) .$$
(10)

The dark matter induced magnetic field is an almost monochromatic signal with frequency  $\nu = \omega/(2\pi)$ . The bandwidth of this signal is determined by the velocity distribution of the dark matter particles. The dark matter velocity dispersion is taken conventionally as  $\Delta v \sim 10^{-3}$ , leading to a bandwidth signal of  $\Delta \nu = v \Delta v \nu \sim 10^{-6} \nu$ . At the same time, within a time scale smaller than the coherent time  $\tau = 1/\Delta \nu \approx 278\,\mathrm{hour}\,\left(\frac{\mathrm{Hz}}{\nu}\right)$ , the dark matter field amplitudes  $a_0$  or  $A_i$  (Eq. (8) and (10)) become stochastically fluctuating [25, 54–56]. As shown later, since our measurement time is much shorter than the coherent time, we can ignore the bandwidth when incorporating this stochastic effect into the analysis [18, 55, 57].

Experimental set-up and data analysis. In our experiment, we employed the QTFM-B scalar atomic magnetometer manufactured by QUSPIN [58]. This instrument is a pulsed, optically pumped rubidium magnetometer that operates based on the Free Induction Decay (FID) detection scheme. The vapor cell contains rubidium atoms that are optically pumped to a polarized state. In the presence of an external magnetic field, these atoms undergo Larmor spin precession at a frequency directly proportional to the magnitude of the applied field. This precession alters the optical absorption and dispersion properties of the atomic vapor, which we detect by measuring the transmission of a 795 nm vertical-cavity surface-emitting laser through the atomic vapor during

the FID signal. The QTFM-B magnetometer can be used to perform a scalar magnetic field measurements at frequencies below 500 Hz. It offers a magnetic field sensitivity below  $20\,\mathrm{pT}/\sqrt{\mathrm{Hz}}$  and supports a maximum data acquisition rate of 1000 samples per second.

The experiment was conducted on 7 August 2025 in the desert of XiaoDushan, located approximately 120 km from Dunhuang City, Gansu Province, China (geographic coordinates: 40.9664° N, 93.9822° E, altitude 1268 m above sea level), as illustrated in Fig. 1. During the measurement, the ambient temperature was recorded at 27 °C, which is within the operational range of the magnetometer. Data collection took place between 12:30 pm and 3:30 pm local time, yielding an effective observation time of  $T_{\rm obs} = 1.05 \,\mathrm{h}$  at a sampling frequency of 62.5 Hz. The magnetometer was connected to a laptop via a 2 m USB cable and controlled using dedicated software that enabled configuration of the sampling rate and calibration of the sensor orientation to avoid the instrument's dead zone. A trial measurement of approximately 30 minutes was first performed to verify the sensor alignment, sampling functionality, and data recording. Subsequently, the main data run was carried out, and the resulting time-series data were recorded on the laptop.

We analyze the data by searching for excess power in the frequency domain, as characterized by the power spectral density (PSD) [54, 59, 60]. The remote desert location of the experiment minimizes dominant anthropogenic noise contributions at low frequencies. The primary source of noise in the recorded data is the magnetometer itself, which we assume to exhibit both Gaussian and stationary behavior throughout the measurement period. Below approximately 0.5 Hz, the noise follows a 1/f power-law dependence, while at higher frequencies, it becomes approximately frequency-independent. Accordingly, we restrict our analysis to the frequency range between 0.1 Hz and 5 Hz. This range is chosen to ensure reliable extraction of magnetic field signals under the condition  $(\omega R_e)^2 < 2$ , where  $\omega$  is the angular frequency and  $R_e$  is the Earth's radius. Within this band, the noise variance is estimated from the power in adjacent frequency bins at each frequency. This approach yields a nearly flat noise background, providing an optimal regime in which narrow spectral features—such as potential signals from ultralight dark matter—can be identified and studied.

The amplitude and thus the PSD of a potential signal at a given frequency is fully determined by Eq. (8) and (10), and can be identified within a background of approximately flat noise. The intrinsic bandwidth of the signal is approximately  $5\times 10^{-6}\,\mathrm{Hz}$ , which is much smaller than the width of a single frequency bin. Specifically, each frequency bin has a resolution of  $1/T_{\mathrm{obs}}=2.8\times 10^{-4}\,\mathrm{Hz}$ , ensuring that the entire signal bandwidth is contained within a single bin. Given the relatively short observation time,  $T_{\mathrm{obs}}\ll \tau=55.6\,\mathrm{hours}\,\big(\frac{5\,\mathrm{Hz}}{\nu}\big)$ , we model the expected dark matter signal as a single narrow

peak appearing in each relevant frequency bin [18].

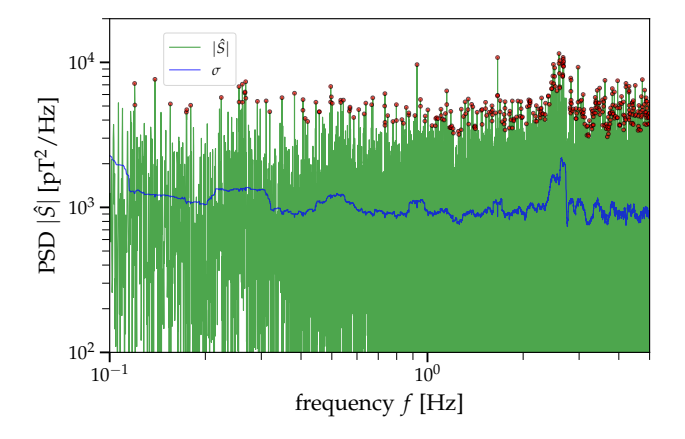


Figure 2. PSD of the observed magnetic fields,  $\hat{S}$  in green, and the standard deviation,  $\sigma$  in blue, evaluated from 200 bins in the immediate vicinity on both sides excluding three center bins. We also marked the naive signal candidates with SNR  $\geq 2$  by circles in red.

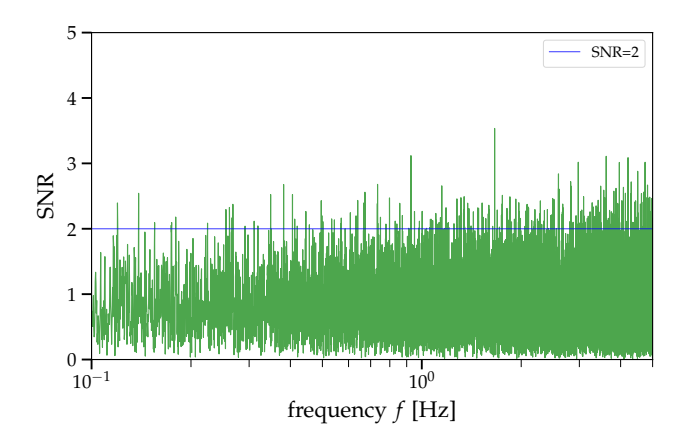


Figure 3. SNR for the frequency of interest. The horizontal solid lines is SNR = 2.

We neglect any cross talk between the PSDs of the signal and noise across all frequencies, as their underlying sources are uncorrelated. Consequently, the single-sided PSD of the measured magnetic field  $\vec{B}(t) = \vec{B}_{\rm n}(t) + \vec{B}_{\rm s}(t)$  at frequency f is given by the sum of the noise and signal contributions [61]:

$$S(f) = S_{n}(f) + S_{s}(f)$$

$$= S_{n}(f) + \frac{2}{T_{obs}} \left| \vec{R}(f_{s}, \mathcal{A}_{s}) \right|^{2} g_{s}^{2} \left\{ \delta(f - f_{s}) \right\}^{2}, (11)$$

where  $S_{\rm n}(f)$  is the PSD of the noise magnetic field  $\vec{B}_{\rm n}(t)$  over the total observation time  $T_{\rm obs}$ , and  $S_{\rm s}(f)$  is the PSD of the signal magnetic field  $\vec{B}_{\rm s}(t)$ , with the signal type denoted by  ${\rm s}=a,\gamma'$  (corresponding to axion and dark photon, respectively). The response function  $\vec{R}(f,\mathcal{A})$  relates

the signal field to the time-domain representation

$$\vec{B}_{\rm s}(t) \equiv \vec{R}(f_{\rm s}, \mathcal{A}_{\rm s}) g_{\rm s} \exp\left(-2\pi i f_{\rm s} t\right) ,$$

with  $g_{a,\gamma'}=g_{a\gamma\gamma}$ ,  $\epsilon$  and  $\mathcal{A}_{a,\gamma'}=a_0$ , A' representing the coupling constants and field amplitudes for axions and dark photons, respectively. The delta function  $\delta(f-f_{\rm s})$  accurately models the line-like spectral signature of the signal for our relatively short observation time  $T_{\rm obs}$ , which is much smaller than the coherent integration time  $\tau$ . Since the noise is statistically stationary within the measurement window in the frequency domain, we define an estimator for the dark matter line signal at frequency  $f=f_{\rm s}$  as

$$\hat{S}(f_{\rm s}) \equiv S_{\rm n}(f_{\rm s}) + 2T_{\rm obs} \left| \vec{R}(f_{\rm s}, \mathcal{A}_{\rm s}) \right|^2 g_{\rm s}^2 , \qquad (12)$$

where we have approximated  $\delta(0) \approx T_{\rm obs}$  for finite observation time. The noise PSD,  $S_{\rm n}(f_{\rm s})$ , follows a  $\chi^2$  distribution with two degrees of freedom [59]. For cases where the observation time exceeds the coherence time, we refer the reader to Refs. [60, 61] for the definition of the weighted estimator applied over multiple data segments, which incorporates the signal bandwidth and corresponding corrections.

We first identify potential signal candidates by calculating the signal-to-noise ratio (SNR), defined as

$$SNR \equiv \sqrt{\frac{\langle \hat{S}(f_{\rm s}) \rangle}{\sigma(f_{\rm s})}} , \qquad (13)$$

where  $\sigma(f_s)$  is the standard deviation of the noise and  $\langle \cdot \rangle$  denotes the ensemble average. The noise standard deviation  $\sigma(f_s)$  is evaluated using the observed PSD over  $\pm 200$  frequency bins centered around  $f=f_s$ , excluding the three bins immediately surrounding  $f=f_s$  to avoid contamination from a potential signal. This approach ensures that the noise variance estimate is independent of any candidate signal itself and automatically excludes signals broader than a single frequency bin [61].

In Fig. 2, we present the amplitude of  $|\hat{S}(f)|$  along with its standard deviation across the frequency range. Across the mass ranges of interest, we identify approximately 300 naive candidates with SNR  $\geq 2$ , but find no candidate exceeding SNR  $\geq 5$  - a threshold commonly associated with discovery claims. The SNR values for the mass ranges of interest are also shown in Fig. 3. Given the absence of statistically significant candidates, we report a null result for the current experiment. A Bayesian statistical framework is employed to interpret the data, and upper limits are placed on the coupling constant  $g_{\rm s}$  as described below.

Performing a change of variables, we define the nor-

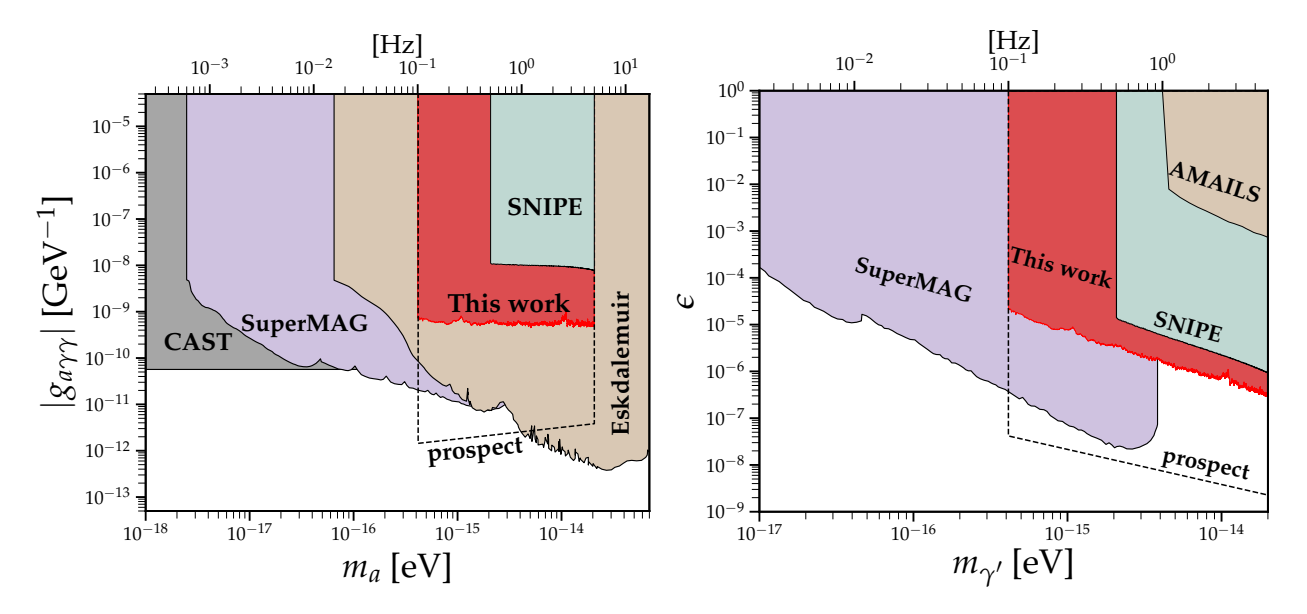


Figure 4. Left: The 95% confidence level (CL) exclusion limit on the axion-photon coupling  $g_{a\gamma\gamma}$  as a function of the axion mass  $m_a$ , derived from the first run of the GPEX experiment. We also display the relevant experimental bounds based on the SuperMAG analysis [51, 62], the SNIPE-hunt analysis [63], the Eskdalemuir observation [61, 64], and the CAST result [20]. The prospective sensitivity, evaluated using a network of 10 magnetometers, each with a sensitivity of 0.54 pT/ $\sqrt{\text{Hz}}$  and operating for one month, is also shown. Right: The 95% CL exclusion limit on the dark photon kinetic-mixing parameter  $\epsilon$  as a function of the dark photon mass  $m_{\gamma'}$ , derived from the first run of the GPEX experiment. We show the limits from the SuperMAG [53, 62] and SNIPE-hunt [63] analyses based on geomagnetic field observations, as well as the limit from the AMAILS experiment [29] based on a synchronized quantum sensor network. The prospective sensitivity is evaluated under the same configuration as for the axion case (i.e., a network of 10 magnetometers, each with 0.54 pT/ $\sqrt{\text{Hz}}$  sensitivity, operating for one month).

malized quantities

$$P = \frac{\hat{S}}{\sigma} \quad \text{and} \quad P_{s} = \frac{2T_{\text{obs}} \left| \vec{R}(f_{s}, \mathcal{A}_{s}) \right|^{2} g_{s}^{2}}{\sigma}, \quad (14)$$

where P represents the normalized excess signal power, and  $P_{\rm s}$  corresponds to the normalized signal PSD. Using these definitions, we apply Bayes' theorem to derive the posterior distribution for the coupling constant  $g_{\rm s}$ . The resulting expression is given by

$$p(P_{s}^{0} \mid P) \propto p(P_{s}^{0}) \int p(P_{s} \mid P_{s}^{0}) \mathcal{L}(P \mid P_{s}) dP_{s}$$

$$= \frac{e^{-P/(1+P_{s}^{0})}}{(1+P_{s}^{0})^{2}}, \qquad (15)$$

where  $\mathcal{L}(P \mid P_s)$  is the likelihood function for the observed power, given by [55, 59],

$$\mathcal{L}(P \mid P_{\rm s}) = e^{-(P+P_{\rm s})} I_0 \left(2\sqrt{PP_{\rm s}}\right) , \qquad (16)$$

and  $I_0$  is the modified Bessel function of the first kind.

Due to the virialized nature of scalar field dark matter, the signal PSD  $P_{\rm s}$  is not deterministic. As discussed previously, on timescales much shorter than the coherence time  $\tau$ , the dark matter field coherently oscillates at

the Compton frequency, causing the amplitude  $A_s$ —and thus the local dark matter density  $\rho$ —to fluctuate around a mean value  $A_s^0 = \sqrt{2\rho_0}/m_s$ , as described in [55, 57]. Consequently, we marginalize the likelihood over the distribution of the excess signal PSD, which is modeled as

$$p(P_{\rm s} \mid P_{\rm s}^0) = \frac{1}{P_{\rm s}^0} e^{-P_{\rm s}/P_{\rm s}^0} ,$$
 (17)

where  $P_{\rm s}^0$  corresponds to the expected signal PSD evaluated at  $\mathcal{A}_{\rm s}=\mathcal{A}_{\rm s}^0$ , i.e.,  $P_{\rm s}^0=P_{\rm s}\big|_{\mathcal{A}_{\rm s}=\mathcal{A}_{\rm s}^0}$ .

The final ingredient required for the posterior is the prior distribution for  $P_s^0$ . Following the approach of [51, 55, 60], we adopt Jeffreys' prior, given by

$$p(P_{\rm s}^0) \propto \frac{1}{1 + P_{\rm s}^0} \ .$$
 (18)

The posterior distribution  $p(P_s^0 \mid P)$  is then properly normalized according to

$$\int_{0}^{\infty} p(P_{s}^{0} \mid P) dP_{s}^{0} = 1.$$
 (19)

For the null search, we derive a 95% confidence level (CL) upper limit on the coupling constant  $g_s$  by solving

the integral equation

$$\int_{0}^{P_{\rm th}} p(P_{\rm s}^{0} \mid P) \, \mathrm{d}P_{\rm s}^{0} = 0.95 \;, \tag{20}$$

where  $P_{\rm th}$  is the threshold value of  $P_{\rm s}^0$  corresponding to the 95% CL. The coupling constant  $g_{\rm s}$  is then obtained from  $P_{\rm th}$  via the relation in Eq. (11). We have verified that, compared to the case where the likelihood in Eq. (16) is used directly (i.e., without marginalizing over the stochastic signal amplitude), the inclusion of the stochastic effects through the marginalized likelihood weakens the resulting constraint by approximately a factor of 2.7, consistent with expectations for our short observation time  $T_{\rm obs} \ll \tau$ , as discussed in [55].

Our results are presented in Fig. 4, which shows the 95% CL exclusion limits on the couplings  $g_{a\gamma\gamma}$  and  $\epsilon$  over the frequency range  $0.1 \leq f \leq 5\,\mathrm{Hz}$ . The corresponding mass range for axion or dark photon dark matter is from  $3.5\times10^{-16}\,\mathrm{eV}$  to  $1.8\times10^{-14}\,\mathrm{eV}$ . In the same figure, we also compare our limits with existing constraints from geomagnetic field observations conducted by the Super-MAG [51, 53, 60, 65], SNIPE-hunt [63], and Eskdalemuir Observatory [61] collaborations, which employed various types of classical magnetometers.

For the axion, our constraint is approximately one order of magnitude stronger than that of the SNIPE-hunt experiment, primarily due to the high sensitivity of our quantum magnetometer. However, our limits are weaker than those from SuperMAG and Eskdalemuir, mainly owing to their significantly longer observation times. The results from the CAST solar axion search [20] are also included in the figure. We note that additional astrophysical observations [66–70], including X-ray observations of the quasar H1821+643 obtained with the Chandra telescope [71], provide even stronger constraints on the axion within the same mass and frequency range.

For the dark photon, our constraint is more sensitive than those from SNIPE-hunt and AMAILS [29], which utilized a synchronized quantum sensor network. However, our limits are not as strong as those from Super-MAG, primarily due to the shorter duration of our observation and the smaller number of magnetometers deployed. Astrophysical constraints [72–74], particularly those derived from dark photon-induced heating and cooling in the gas-rich Leo T dwarf galaxy [75], yield the most stringent limits. Nevertheless, these astrophysical bounds rely strongly on the inferred cooling rates of the relevant systems and the detailed understanding of the underlying cooling mechanisms.

Conclusion. In this work, we present the first geomagnetic observations conducted by the GPEX collaboration to search for axion and dark photon dark matter signals within the Earth's cavity, arising from their interactions with the geomagnetic field. Operating at a remote experimental site isolated from anthropogenic elec-

tromagnetic interference and employing a highly sensitive quantum magnetometer, we performed a one-hour observation that reached the intrinsic noise floor of the instrument. No robust signal was observed, the data were analyzed within a Bayesian framework to derive constraints on the axion-photon and dark photon-photon couplings. Remarkably, by using a single atomic magnetometer and only one hour of measurement, we achieved a sensitivity exceeding that of the SNIPE-Hunt experiment.

We aim to surpass the SuperMAG and Eskdalemuir limits derived from long-term monitoring by conducting extended observations with more sensitive quantum magnetometers. As the current experimental reach is constrained by magnetometer sensitivity rather than geomagnetic noise, we plan to establish a high-performance network of quantum magnetometers to search for dark matter signals and potentially exceed existing astrophysical bounds. Such a network can enhance the effective sensitivity and, through correlated measurements, enable confident discrimination of dark matter signals from various noise sources [29, 45, 76–78]. For instance, employing 10 quantum magnetometers with sensitivity of 0.54  $pT/\sqrt{Hz}$  [79], improved by a factor of 40, could enhance the overall sensitivity by about three orders of magnitude after one month of integration, as shown in Fig. 4. In the higher-frequency regime, signal model predictions are available [80], allowing our search to be extended beyond the low-frequency range. Furthermore, as mentioned in [63], employing local multi-sensor arrays to measure the curl of the local magnetic field can extend the accessible frequency range to approximately 1 kHz.

**Acknowledgement**. This work is supported by the National Key Research and Development Program of China (Grant No. 2022YFA1605000), and Quantum Science and Technology-National Science and Technology Major Project (Grant No. 2024ZD0302300). L.W. is supported by the NNSFC under Grant No. 12275134 and No. 12335005. J.S. is supported by Peking University under startup Grant No. 7101302974 and the National Natural Science Foundation of China (NNSFC) under Grants No. 12025507, No.12450006. J.G. is supported by the NNSFC under Grant No. 12305111. B.Z. is supported by the NNSFC under Grant No. 12275232 and Shangdong Provincial Natural Science Foundation for Distinguished Young Scholars under Grant No. ZR2025QA20. Q.Y. is supported by the Project for Young Scientists in Basic Research of Chinese Academy of Sciences under Grant No. YSBR-061.

These authors contribute equally

<sup>†</sup> corresponding author: jshu@pku.edu.cn

corresponding author: weikai@buaa.edu.cn

<sup>§</sup> corresponding author: leiwu@njnu.edu.cn (project CI)

<sup>¶</sup> corresponding author: zhubin@mail.nankai.edu.cn

- J. Silk et al., Particle Dark Matter: Observations, Models and Searches, edited by G. Bertone (Cambridge Univ. Press, Cambridge, 2010).
- [2] J. Preskill, M. B. Wise, and F. Wilczek, Phys. Lett. B 120, 127 (1983).
- [3] L. Abbott and P. Sikivie, Phys. Lett. B 120, 133 (1983).
- [4] M. Dine and W. Fischler, Phys. Lett. B 120, 137 (1983).
- [5] A. E. Nelson and J. Scholtz, Phys. Rev. D 84, 103501 (2011), arXiv:1105.2812 [hep-ph].
- [6] P. Arias, D. Cadamuro, M. Goodsell, J. Jaeckel, J. Redondo, and A. Ringwald, JCAP 06, 013 (2012), arXiv:1201.5902 [hep-ph].
- [7] J. Jaeckel, Frascati Phys. Ser. 56, 172 (2012), arXiv:1303.1821 [hep-ph].
- [8] R. D. Peccei and H. R. Quinn, Phys. Rev. Lett. 38, 1440 (1977)
- [9] A. Arvanitaki, S. Dimopoulos, S. Dubovsky, N. Kaloper, and J. March-Russell, Phys. Rev. D 81, 123530 (2010), arXiv:0905.4720 [hep-th].
- [10] P. Svrcek and E. Witten, JHEP 06, 051 (2006), arXiv:hep-th/0605206.
- [11] S. A. Abel, M. D. Goodsell, J. Jaeckel, V. V. Khoze, and A. Ringwald, JHEP 07, 124 (2008), arXiv:0803.1449 [hep-ph].
- [12] B. Holdom, Phys. Lett. B 166, 196 (1986).
- [13] K. R. Dienes, C. F. Kolda, and J. March-Russell, Nucl. Phys. B 492, 104 (1997), arXiv:hep-ph/9610479.
- [14] S. A. Abel, J. Jaeckel, V. V. Khoze, and A. Ringwald, Phys. Lett. B 666, 66 (2008), arXiv:hep-ph/0608248.
- [15] M. Goodsell, J. Jaeckel, J. Redondo, and A. Ringwald, JHEP 11, 027 (2009), arXiv:0909.0515 [hep-ph].
- [16] P. W. Graham, J. Mardon, and S. Rajendran, Phys. Rev. D 93, 103520 (2016), arXiv:1504.02102 [hep-ph].
- [17] R. Bradley, J. Clarke, D. Kinion, L. J. Rosenberg, K. van Bibber, S. Matsuki, M. Muck, and P. Sikivie, Rev. Mod. Phys. 75, 777 (2003).
- [18] D. Budker, P. W. Graham, M. Ledbetter, S. Rajendran, and A. Sushkov, Phys. Rev. X 4, 021030 (2014), arXiv:1306.6089 [hep-ph].
- [19] H. An, M. Pospelov, and J. Pradler, Phys. Rev. Lett. 111, 041302 (2013), arXiv:1304.3461 [hep-ph].
- [20] V. Anastassopoulos et al. (CAST), Nature Phys. 13, 584 (2017), arXiv:1705.02290 [hep-ex].
- [21] T. Braine et al. (ADMX), Phys. Rev. Lett. 124, 101303 (2020), arXiv:1910.08638 [hep-ex].
- [22] A. V. Gramolin, D. Aybas, D. Johnson, J. Adam, and A. O. Sushkov, Nature Phys. 17, 79 (2021), arXiv:2003.03348 [hep-ex].
- [23] C. Smorra et al., Nature 575, 310 (2019), arXiv:2006.00255 [physics.atom-ph].
- [24] M. Jiang, H. Su, A. Garcon, X. Peng, and D. Budker, Nature Phys. 17, 1402 (2021), arXiv:2102.01448 [hep-ph].
- [25] Y. Chen, M. Jiang, J. Shu, X. Xue, and Y. Zeng, Phys. Rev. Res. 4, 033080 (2022), arXiv:2111.06732 [hep-ph].
- [26] E. Aprile et al. (XENON), Phys. Rev. Lett. 129, 161805 (2022), arXiv:2207.11330 [hep-ex].
- [27] I. M. Bloch, R. Shaham, Y. Hochberg, E. Kuflik, T. Volansky, and O. Katz, Nature Commun. 14, 5784 (2023), arXiv:2209.13588 [hep-ph].
- [28] K. Wei et al., Rept. Prog. Phys. 88, 057801 (2025), arXiv:2306.08039 [hep-ph].
- [29] M. Jiang et al., Nature Commun. 15, 3331 (2024), arXiv:2305.00890 [quant-ph].
- [30] A. Arza, Q. Guo, L. Wu, Q. Yang, X. Yang, Q. Yuan,

- and B. Zhu, Sci. Bull. **69**, 2971 (2024), arXiv:2309.06857 [hep-ph].
- [31] H. An, X. Chen, S. Ge, J. Liu, and Y. Luo, Nature Commun. 15, 915 (2024), arXiv:2301.03622 [hep-ph].
- [32] D. Gavilan-Martin et al., Nature Commun. 16, 4953 (2025), arXiv:2408.02668 [hep-ph].
- [33] L. Brouwer et al. (DMRadio), Phys. Rev. D 106, 103008 (2022), arXiv:2204.13781 [hep-ex].
- [34] C. P. Salemi et al., Phys. Rev. Lett. 127, 081801 (2021), arXiv:2102.06722 [hep-ex].
- [35] D. F. J. Kimball and K. van Bibber, eds., The Search for Ultralight Bosonic Dark Matter (Springer, 2023).
- [36] P. Sikivie, Rev. Mod. Phys. 93, 015004 (2021), arXiv:2003.02206 [hep-ph].
- [37] I. G. Irastorza and J. Redondo, Prog. Part. Nucl. Phys. 102, 89 (2018), arXiv:1801.08127 [hep-ph].
- [38] J. Berger and A. Bhoonah, (2022), arXiv:2206.06364 [hep-ph].
- [39] A. V. Dixit, S. Chakram, K. He, A. Agrawal, R. K. Naik, D. I. Schuster, and A. Chou, Phys. Rev. Lett. 126, 141302 (2021), arXiv:2008.12231 [hep-ex].
- [40] A. Agrawal, A. V. Dixit, T. Roy, S. Chakram, K. He, R. K. Naik, D. I. Schuster, and A. Chou, Phys. Rev. Lett. 132, 140801 (2024), arXiv:2305.03700 [quant-ph].
- [41] R. Cervantes et al., Phys. Rev. D 110, 043022 (2024), arXiv:2208.03183 [hep-ex].
- [42] Z. Tang et al. (SHANHE), Phys. Rev. Lett. 133, 021005 (2024), arXiv:2305.09711 [hep-ex].
- [43] Y. Zeng et al. (SHANHE), Sci. Bull. 70, 661 (2025), arXiv:2402.03432 [hep-ph].
- [44] P. Zheng et al., (2025), arXiv:2507.23538 [quant-ph].
- [45] S. Afach et al., Nature Phys. 17, 1396 (2021), arXiv:2102.13379 [astro-ph.CO].
- [46] Y. Chen, M. Jiang, Y. Ma, J. Shu, and Y. Yang, Phys. Rev. Res. 4, 023015 (2022), arXiv:2103.12085 [hep-ph].
- [47] K. Wurtz, B. M. Brubaker, Y. Jiang, E. P. Ruddy, D. A. Palken, and K. W. Lehnert, PRX Quantum 2, 040350 (2021), arXiv:2107.04147 [quant-ph].
- [48] Y. Chen, C. Li, Y. Liu, J. Shu, Y. Yang, and Y. Zeng, Rept. Prog. Phys. 88, 057601 (2025), arXiv:2309.12387 [hep-ph].
- [49] Y. Jiang, E. P. Ruddy, K. O. Quinlan, M. Malnou, N. E. Frattini, and K. W. Lehnert, PRX Quantum 4, 020302 (2023), arXiv:2211.10403 [quant-ph].
- [50] K. M. Backes et al. (HAYSTAC), Nature 590, 238 (2021), arXiv:2008.01853 [quant-ph].
- [51] A. Arza, M. A. Fedderke, P. W. Graham, D. F. J. Kimball, and S. Kalia, Phys. Rev. D 105, 095007 (2022), arXiv:2112.09620 [hep-ph].
- [52] P. Alken, E. Thébault, C. D. Beggan, H. Amit, J. Aubert, J. Baerenzung, T. Bondar, W. Brown, S. Califf, A. Chambodut, et al., Earth, Planets and Space 73, 1 (2021).
- [53] M. A. Fedderke, P. W. Graham, D. F. J. Kimball, and S. Kalia, Phys. Rev. D 104, 075023 (2021), arXiv:2106.00022 [hep-ph].
- [54] A. Derevianko, Phys. Rev. A 97, 042506 (2018), arXiv:1605.09717 [physics.atom-ph].
- [55] G. P. Centers et al., Nature Commun. 12, 7321 (2021), arXiv:1905.13650 [astro-ph.CO].
- [56] H. Nakatsuka, S. Morisaki, T. Fujita, J. Kume, Y. Michimura, K. Nagano, and I. Obata, Phys. Rev. D 108, 092010 (2023), arXiv:2205.02960 [astro-ph.CO].
- [57] C. A. J. O'Hare and A. M. Green, Phys. Rev. D 95,

- 063017 (2017), arXiv:1701.03118 [astro-ph.CO].
- [58] https://quspin.com/qtfm-gen-2.
- [59] E. J. Groth, Astrophys. J. Supp. 29, 285 (1975).
- [60] M. A. Fedderke, P. W. Graham, D. F. Jackson Kimball, and S. Kalia, Phys. Rev. D 104, 095032 (2021), arXiv:2108.08852 [hep-ph].
- [61] A. Nishizawa, A. Taruya, and Y. Himemoto, (2025), arXiv:2504.07559 [hep-ph].
- [62] M. Friel, J. W. Gjerloev, S. Kalia, and A. Zamora, Phys. Rev. D 110, 115036 (2024), arXiv:2408.16045 [hep-ph].
- [63] I. A. Sulai et al., Phys. Rev. D 108, 096026 (2023), arXiv:2306.11575 [hep-ph].
- [64] A. Taruya, A. Nishizawa, and Y. Himemoto, (2025), arXiv:2504.06653 [hep-ph].
- [65] A. Arza, Y. Gong, J. Shu, L. Wu, Q. Yuan, and B. Zhu, (2025), arXiv:2501.14949 [hep-ph].
- [66] G.-W. Yuan, Z.-Q. Xia, C. Tang, Y. Zhao, Y.-F. Cai, Y. Chen, J. Shu, and Q. Yuan, JCAP 03, 018 (2021), arXiv:2008.13662 [astro-ph.HE].
- [67] A. Caputo, H.-T. Janka, G. Raffelt, and E. Vitagliano, Phys. Rev. Lett. 128, 221103 (2022), arXiv:2201.09890 [astro-ph.HE].
- [68] D. Wouters and P. Brun, Astrophys. J. 772, 44 (2013), arXiv:1304.0989 [astro-ph.HE].
- [69] C. Dessert, J. W. Foster, and B. R. Safdi, Phys. Rev. Lett. 125, 261102 (2020), arXiv:2008.03305 [hep-ph].
- [70] M. C. D. Marsh, H. R. Russell, A. C. Fabian, B. P. Mc-Namara, P. Nulsen, and C. S. Reynolds, JCAP 12, 036

- (2017), arXiv:1703.07354 [hep-ph].
- [71] J. S. Reynés, J. H. Matthews, C. S. Reynolds, H. R. Russell, R. N. Smith, and M. C. D. Marsh, Mon. Not. Roy. Astron. Soc. 510, 1264 (2021), arXiv:2109.03261 [astro-ph.HE].
- [72] E. Fischbach, H. Kloor, R. A. Langel, A. T. Y. Liu, and M. Peredo, Phys. Rev. Lett. 73, 514 (1994).
- [73] G. Marocco, (2021), arXiv:2110.02875 [hep-ph].
- [74] A. Bhoonah, J. Bramante, F. Elahi, and S. Schon, Phys. Rev. D 100, 023001 (2019), arXiv:1812.10919 [hep-ph].
- [75] D. Wadekar and G. R. Farrar, Phys. Rev. D 103, 123028 (2021), arXiv:1903.12190 [hep-ph].
- [76] M. Pospelov, S. Pustelny, M. P. Ledbetter, D. F. Jackson Kimball, W. Gawlik, and D. Budker, Phys. Rev. Lett. 110, 021803 (2013), arXiv:1205.6260 [hep-ph].
- [77] A. Derevianko and M. Pospelov, Nature Phys. 10, 933 (2014), arXiv:1311.1244 [physics.atom-ph].
- [78] B. M. Roberts, G. Blewitt, C. Dailey, M. Murphy, M. Pospelov, A. Rollings, J. Sherman, W. Williams, and A. Derevianko, Nature Commun. 8, 1195 (2017), arXiv:1704.06844 [hep-ph].
- [79] X. Huang, W. Wang, Y. Hu, Y.-C. Liu, J. Fang, and K. Wei, Phys. Rev. Lett. 135, 043001 (2025).
- [80] A. Taruya, A. Nishizawa, and Y. Himemoto, (2025), arXiv:2509.14673 [hep-ph].
- [81] M. Tanabashi et al. (Particle Data Group), Phys. Rev. D 98, 030001 (2018).

## Supplementary Materials: Search for Ultralight Dark Matter with Quantum Magnetometry in the Earth's Cavity

Ariel Arza, 1,2 Yuanlin Gong, 1 Jun Guo, 3 Xiaofei Huang, 4 Jing Shu, 5,6,7 Hongliang Tian, 1 Wenyu Wang, 8 Kai Wei, 4,9 Lei Wu, 1,2 Mingming Xia, 10 Jin Min Yang, 11,12 Qiang Yuan, 13,14 Yang Zhang 11 Yi Zhang, 13,14 Bin Zhu, 2 Department of Physics and Institute of Theoretical Physics, Nanjing Normal University, Nanjing, 210023, China <sup>2</sup>Nanjing Key Laboratory of Particle Physics and Astrophysics, Nanjing, 210023, China <sup>3</sup> College of Physics and Communication Electronics, Jiangxi Normal University, Nanchang 330022, China <sup>4</sup>School of Instrumentation and Optoelectronic Engineering, Beihang University, Beijing 100191, China <sup>5</sup>School of Physics and State Key Laboratory of Nuclear Physics and Technology, Peking University, Beijing 100871, China <sup>6</sup>Center for High Energy Physics, Peking University, Beijing 100871, China <sup>7</sup>Beijing Laser Acceleration Innovation Center, Huairou, Beijing, 101400, China <sup>8</sup>Beijing University of Technology, 100124, Beijing, China <sup>9</sup>Quantum Science and Technology College, Beihang University, Beijing 100191, China <sup>10</sup>Hangzhou Institute of Extremely-Weak Magnetic Field Major National Science and Technology Infrastructure, Hangzhou, 310051, China <sup>11</sup> Center for Theoretical Physics, Henan Normal University, Xinxiang 453007, China <sup>12</sup>Institute of Theoretical Physics, Chinese Academy of Sciences, Beijing 100190, China <sup>13</sup>Key Laboratory of Dark Matter and Space Astronomy, Purple Mountain Observatory, Chinese Academy of Sciences, Nanjing 210023, China <sup>14</sup>School of Astronomy and Space Science, University of Science and Technology of China, Hefei 230026, China <sup>15</sup>School of Physics, Yantai University, Yantai 264005, China

## DISTRIBUTION OF THE NOISE AMPLITUDE

As discussed in the main text, the noise power spectral density (PSD) follows a  $\chi^2$  distribution with two degrees of freedom (dof). The flat noise behavior across our frequency range of interest allows us to study the distribution of noise amplitudes and estimate the noise variance using the PSD values of neighboring frequency bins. In Fig. S1, we show the distributions of the observed PSD within  $\pm 200$  frequency bins around  $f = f_s$ , excluding the three bins centered on  $f_s$ , where  $f_s$  denotes the expected signal frequency. For the six representative frequencies—1.3631, 1.4705, 1.4797, 1.6101, 2.1342, and 3.3608 Hz—the distributions are well described by a  $\chi^2$  distribution with a dof close to two, as shown in each subplot. We also present the p-values from the  $\chi^2$  goodness-of-fit test [81] and the corresponding scale parameters in the same figure. Furthermore, Fig. S2 shows the p-values of the goodness-of-fit test across the entire frequency range of interest.

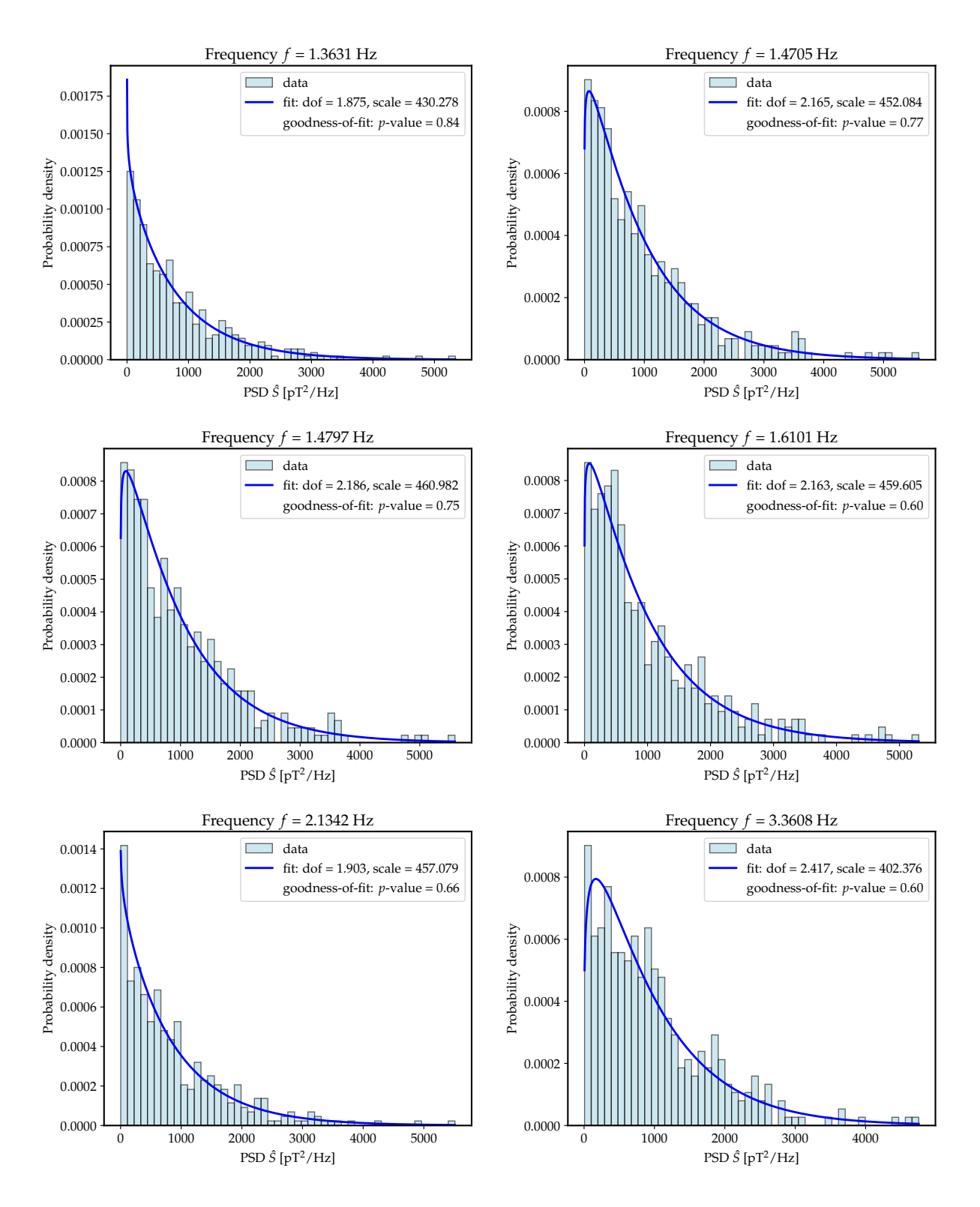


Figure S1. Six representative noise amplitude distributions from observed PSD at specific frequencies. The blue curves denote the best-fit  $\chi^2$  distributions, along with the corresponding fitted dofs, scale parameters, and p-values from the goodness-of-fit test.

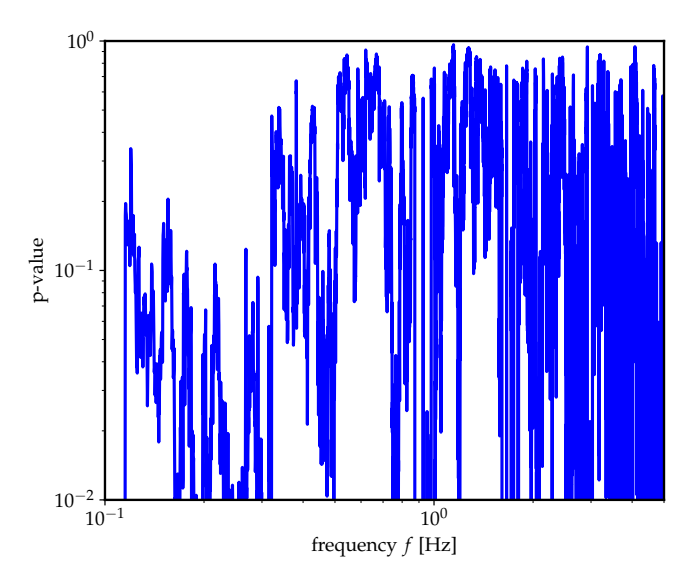


Figure S2. p-value from the  $\chi^2$  goodness-of-fit test for the frequency range of interest, 0.1 Hz to 5 Hz.